Journal of Catalysis 272 (2010) 37–43

Contents lists available at ScienceDirect

Journal of Catalysis

journal homepage: www.elsevier.com/locate/jcat

Hierarchical SAPO-5 catalysts active in acid-catalyzed reactions

Nadiya Danilina [a], Frank Krumeich [b], Jeroen A. van Bokhoven [a,*]

[a] ETH Zurich, Institute for Chemical and Bioengineering, Wolfgang-Pauli-Str. 10, 8093 Zurich, Switzerland
[b] ETH Zurich, Laboratory of Inorganic Chemistry, Wolfgang-Pauli-Str. 10, 8093 Zurich, Switzerland

ARTICLE INFO

Article history:
Received 2 February 2010
Revised 17 March 2010
Accepted 17 March 2010
Available online 18 April 2010

Keywords:
SAPO-5
Hierarchical
Mesoporous
Bimodal
Alkylation

ABSTRACT

Crystalline silicoaluminophosphate (SAPO) of the AFI framework type with a bimodal pore system and high silicon content was hydrothermally synthesized using a soft template with a silicon-containing head group and cyclohexylamine to maintain microporosity. The structural and catalytic properties of the hierarchical structure were extensively characterized and compared to those of microporous SAPO-5 and H-ZSM-5. Temperature-programmed desorption of *n*-propylamine, isomerization of 2-methyl-2-pentene, and monomolecular cracking of propane indicated a large number of Brønsted acid sites and their high reactivity, similar to those of microporous H-SAPO-5. The catalytic activity of the hierarchical H-SAPO-5 was much higher in space-demanding alkylation of benzene with benzyl alcohol. At 353 K and under autogenous pressure, the conversion of benzyl alcohol over the hierarchical sample reached 98%, whereas the conversion over the microporous H-SAPO-5 was around 66% and over H-ZSM-5 below 10%. In contrast to H-ZSM-5, the external surfaces of H-SAPO-5 and H-SAPO-5M contribute to the alkylation reaction. Other procedures to yield mesoporous SAPO, such as hard-templating with carbon, soft-templating with amphiphilic surfactants, and phosphorus- or aluminum-containing molecules, resulted in impure, amorphous, non-mesoporous, or much less acidic materials.

1. Introduction

Silicoaluminophosphates (SAPO) have considerable potential as acidic catalyst for the conversion of hydrocarbons. Microporous SAPO-5 is active in cumene synthesis [1], xylene isomerization [2], toluene alkylation by methanol [3], isopropylation of benzene [4], transalkylation of toluene with trimethylbenzenes [5], and many other reactions. SAPO-5 is a 12-membered ring, wide-pore zeolite with a pore size of 7.3 × 7.3 Å. However, mesoporous or hierarchical SAPOs could increase the external surface area and offer more space for bulky molecules to diffuse and react. Unlike aluminosilicate zeolites, for which various methods exist to create mesopores, little is known about the generation of mesopores in SAPOs. Some mesoporous SAPO structures have been synthesized [6–9], but their catalytic properties have not been studied in depth.

The most important methods to synthesize mesoporous zeolites and zeotypes are soft-templating [10], hard-templating [11], pillaring/delamination [12], post-synthesis treatment [13], and use of zeolite seeds as precursors in the preparation of mesoporous structures [14]. Mesoporous zeolites, which have the most desirable properties for catalysis, such as high crystallinity, narrow pore size distribution, uniform pores, hydrothermal stability, and zeolite-like acidity, have been reported. Using a template enables the control of the shape and size of the solid and its pore system. Recently, a new type of soft template for the synthesis of mesoporous zeolites, such as ZSM-5 [9,15,16] and SAPO [8,17], has been described. These so-called porogenes are surfactant molecules; they contain silicon that enhances the interaction of the template with the growing zeolite crystals and prevents phase segregation during crystallization. Zeolites and zeotypes of high crystallinity and with a hierarchical pore structure were obtained. It was shown that such hierarchical materials have considerable catalytic potential [8,16,18–20].

Based on these original ideas, we designed a method to synthesize microcrystalline SAPO with a high silicon content and bimodal pore system using a soft template with a silicon-containing head group [9] and an additional template cyclohexylamine to create microporosity. We compared this method to alternative procedures of obtaining mesoporous SAPO, such as a soft-templating with phosphorus- and aluminum-containing molecules and amphiphilic surfactants and a hard-templating with carbon nanoparticles. The catalytic activity of the hierarchical H-SAPO-5 was evaluated in the liquid-phase alkylation of benzene with benzyl alcohol, in monomolecular propane cracking, and in the isomerization of 2-methyl-2-pentene. The monomolecular cracking of propane yields the intrinsic reactivity of the Brønsted acid sites [21–23]. The apparent activation barrier is a combined measure of the heat of adsorption and the energy required to transfer the proton from the zeolite to the alkane. The isomerization of 2-methyl-2-pentene is a probe reaction to evaluate the acidity of solid acids [24]. The molar ratio of *trans*-3-methyl-2-pentene,

* Corresponding author.
E-mail address: j.a.vanbokhoven@chem.ethz.ch (J.A. van Bokhoven).

0021-9517/$ - see front matter © 2010 Elsevier Inc. All rights reserved.
doi:10.1016/j.jcat.2010.03.014

obtained by the methyl shift, to *trans*- and *cis*-4-methyl-2-pentene, obtained by the hydrogen shift reflects the acidity. The alkylation of benzene with benzyl alcohol is a space-requiring acid-catalyzed reaction, which allows the determination of active sites in the large pores.

2. Experimental

2.1. Catalyst preparation

2.1.1. Microporous SAPO-5

Microporous SAPO-5 was hydrothermally synthesized from a gel consisting of Al_2O_3:P_2O_5:0.24SiO_2:0.15cyclohexylamine:20H_2O. During preparation, 6.808 g aluminum isopropoxide (Fluka, >98%) was mixed with 3.27 g orthophosphoric acid (Merck, 85%), dissolved in 14 g of deionized water, and stirred for 1 h. A solution of 0.99 g of cyclohexylamine was dissolved in 10 g of deionized water and stirred for 1 h. Both solutions were then mixed and stirred for another hour. Finally, 0.96 g of silica aerosol Cab-osil M-5 (Riedel-de-Haën) was added, and the mixture was stirred for 2 h. The gel was crystallized in 60-mL PEEK-lined stainless-steel autoclaves at 473 K for 2 h and subsequently for 22 h at 463 K. The product was recovered by filtration, washed with 2 L of deionized water, dried at room temperature, and calcined in air at 823 K for 20 h to remove the template. The sample was ion-exchanged three times with 1 M NH_4NO_3 (Fluka, >99%) for 2 h at 348 K and calcined in nitrogen at 723 K for 4 h to give H-SAPO-5.

2.1.2. Mesoporous SAPO-5

2.1.2.1. Soft-templating with organosilane. The synthesis procedure was analogous to that of SAPO-5, with the exception that [3-(trimethoxysilyl)propyl]hexadecyldimethylammonium chloride (TPHAC) was additionally used as a template to generate mesopores. A solution of 1.91 g TPHAC was added to the aqueous solution of cyclohexylamine and stirred overnight before it was mixed with the aluminophosphate solution. TPHAC was synthesized according to a reported procedure [25]. The composition of the gel of the hierarchical SAPO-5M was Al_2O_3:P_2O_5:0.24SiO_2:0.15cyclohexylamine:0.009TPHAC:20H_2O. The templates were removed by calcination (see Section 2.1.1), and ion-exchange was performed according to the procedure described earlier. The calcined sample was labeled H-SAPO-5M.

2.1.2.2. Soft-templating with a phosphorus-containing molecule. H-SAPO-P was prepared in the same way as H-SAPO-5M. Instead of TPHAC, a mixture of 2.4 g of mono-*n*-dodecylphosphate (Alfa Aesar) in 1 mL ethanol was added.

2.1.2.3. Soft-templating with an aluminum-containing molecule. SAPO-A was hydrothermally synthesized from a gel mixture of composition Al_2O_3:1.73P_2O_5:1.21SiO_2:1.03Al-dihydroxo-monoheptadecylester:209.72H_2O. A solution of 2.512 g aluminum isopropoxide (Fluka, >98%) in 5.825 g deionized water was mixed with 2.451 g orthophosphoric acid (Merck, 85%), dissolved in 5.01 g of deionized water, and stirred for 1.5 h. A solution of 4.304 g of aluminum-dihydroxo-mono-heptadecylester (Fluka, technical grade) was suspended in 5.032 g of deionized water, added to the aluminophosphate solution, and stirred for 1.5 h. Finally, 1.7426 g of tetraethylorthosilicate (Fluka, >98%) was added and the mixture was stirred overnight. The gel was crystallized in 60-mL PEEK-lined stainless-steel autoclaves at 473 K for 20 h. The product was recovered by filtration, washed with 2 L of deionized water, dried at room temperature, and calcined in air at 823 K for 20 h to remove the template.

2.1.2.4. Soft-templating with amphiphilic surfactant. H-SAPO-S was prepared in the same way as H-SAPO-5M. Instead of TPHAC, a mixture of 1.01 g of dodecyltrimethylammonium bromide (Fluka, >98%) and 1.14 g of tetramethylammonium hydroxide (Fluka, 25% in water) was added.

2.1.2.5. Hard-templating with carbon black. SAPO-C was synthesized as in Ref. [26]. A mixture of 2.04 g of aluminum isopropoxide and 7 mL THF was impregnated onto 1 g of carbon (Black Pearls 2000, CABOT), which had an average particle diameter of about 12 nm. The carbon black was dried at 383 K for 24 h prior to use. The carbonaceous material was left to dry at room temperature in a flow of air for 6 h. A solution of 1.5 g phosphoric acid, 1.62 g triethylamine, and 0.27 g hydrofluoric acid (Fluka, 48 wt.%) in 1 mL of deionized water was prepared and stirred for 1 h. The dry carbon material was impregnated with this solution and subsequently with 0.87 g of TEOS (Fluka, >98%). Then, the material was put into an open 10-mL Teflon bottle and placed in the PEEK liner filled with 20 mL of deionized water. The gel was hydrothermally crystallized in a stainless-steel autoclave at 448 K for three days, after which the product was filtered, washed with 2 L deionized water, and dried at 353 K overnight in a vacuum oven. The sample was calcined for 20 h at 873 K with a heating rate of 1 K/min in a flow of air. SAPO-C was ion-exchanged to obtain H-SAPO-C after calcination.

2.2. Characterization

X-ray powder diffraction (XRD) was conducted on a STOE STADI-P2 diffractometer in transmission mode using a flat sample holder and Ge-monochromated Cu $K\alpha_1$ radiation. The instrument was equipped with a position-sensitive detector with a resolution of $\sim 0.01^\circ$ in 2θ.

Nitrogen sorption measurements were performed at the temperature of liquid nitrogen on a Tristar 3000 apparatus of Micromeritics. Prior to the measurements, the samples were degassed at 10 Pa and 523 K for at least 2 h. The surface area was determined by the BET method; the *t*-plot method was used to determine the specific pore volume.

Atomic absorption spectroscopy (AAS) was performed on a Varian SpectrAA 220 FS spectrometer to determine elemental constitution. The samples were dissolved in an HF/HNO_3/water matrix overnight. Quantification of the aluminum content was done by the standard addition method. For silicon, individual calibration curves were measured and used for quantification.

^{27}Al magic-angle spinning nuclear magnetic resonance (MAS NMR) experiments were carried out on a Bruker Avance 700 NMR spectrometer using a 2.5-mm double-resonance probe-head. The resonance frequency for ^{27}Al was 182.4 MHz and the pulse length was 6 μs. The recycle delay was 1 s. All spectra were obtained at a spinning speed of 15 kHz. The ^{27}Al chemical shifts were referenced to Alum ($(NH_4)Al(SO_4)_2{\cdot}12H_2O$). ^{29}Si and ^{31}P MAS NMR measurements were performed on a Bruker Avance 500 NMR spectrometer using a 4-mm probe-head. For ^{29}Si MAS NMR, a spinning frequency of 8 kHz and a relaxation delay of 10 s were employed. The ^{29}Si chemical shifts were referenced to octakis-(trimethylsiloxy)silsesquioxane. To record the ^{31}P MAS NMR spectra, a spinning frequency of 8 kHz and a relaxation delay of 1 s were employed. The field was calibrated by measuring ^{13}C MAS NMR of glycine.

Scanning electron microscopy (SEM) was performed on a LEO 1530 Gemini instrument (Zeiss) operated at 1 kV. The sample was deposited onto a conductive carbon foil supported on an aluminum stub. Transmission electron micrographs (TEM) were obtained on a Philips CM30 microscope with a point resolution of 0.2 nm at 300 kV. For TEM, the sample was ground, dispersed in ethanol, and deposited on a holey carbon film supported on a copper grid.

For the temperature-programmed desorption of propylamine with thermogravimetric analysis (TPD–TGA), approximately 20 mg sample were activated overnight at a pressure below 10^{-4} Pa by heating to 723 K with a ramp of 2 K/min. The sample was then exposed to *n*-propylamine at 473 K for 2 h and cooled to room temperature. The sample was evacuated for about 2 h to remove physisorbed *n*-propylamine. The thermogravimetric decomposition of *n*-propylamine was performed with a heating rate of 10 K/min and in a flow of 20 mL/min Ar in a Mettler Toledo TGA/SDTA851e instrument. The amount of decomposed *n*-propylamine was obtained from the mass change in the TGA curves between 573 and 650 K.

2.3. Catalytic tests

2.3.1. Propane cracking

The monomolecular propane cracking was performed in a setup with six parallel-flow tubular quartz reactors. Ten percent propane in argon was reacted between 723 and 873 K at 100 kPa total pressure. About 100 mg of the catalyst was activated in a reactor in 10% oxygen in argon at 878 K for 1 h with a heating ramp of 2 K/min. A volumetric flow of 5 mL/min per reactor was used to keep the conversion below 5%. The products were analyzed in the effluent gas stream with an on-line Agilent 3000 MicroGC gas chromatograph equipped with MolSieve 5A, PLOT U, and Alumina PLOT columns. The procedure to determine the catalyst performance is described in more detail elsewhere [21,19,23].

2.3.2. Isomerization of 2-methyl-2-pentene

The gas phase isomerization of 2-methyl-2-pentene (2M2P) [24] was studied in a plug-flow reactor. A concentration of 0.1 g of the catalyst was pretreated in flowing helium for about 1 h at 723 K prior to the reaction. The reaction was initially conducted at 473 K for 1 h, while a flow of 15 mL/min of 7 vol.% 2M2P in helium at atmospheric pressure was passed over the catalyst. The feed was then switched to helium and the catalyst cooled to 448 K and then to 423 K. The samples were taken 10 min after switching on the feed at 473, 448, and 423 K. The products were analyzed on-line with an Agilent 6890 GC with an FID detector using a 50-m HP5 packed column.

2.3.3. Alkylation of benzene with benzyl alcohol

Alkylation of benzene with benzyl alcohol was performed in 25-mL Berghof autoclaves BR-25. A concentration of 0.11 g of the catalyst was activated *ex situ* at 523 K in a flow of nitrogen, transferred to the reactor in a flow of nitrogen, and covered with 14.9 g benzene (Sigma–Aldrich, puriss.), which was dried over a mol sieve (ZEOCHEM® Purmol from Uetikon Chemie AG). Benzyl alcohol (0.26 g) (Fluka, puriss.) was added, resulting in a molar ratio of benzene to benzyl alcohol of around 80. The reactor was purged with nitrogen and a permanent pressure of 25–27 bars was maintained during the reaction to keep the reactants in the liquid phase at the reaction temperature of 433 K. The mixture was stirred at 1250 rpm throughout the run, which was determined to be sufficiently fast. Small liquid samples were withdrawn periodically and analyzed using a GC–MS setup equipped with a capillary HP-PONA (Agilent Technologies) column.

3. Results

3.1. Synthesis and characterization

Fig. 1 shows X-ray diffractograms of SAPO-5, SAPO-5M, SAPO-P, SAPO-A, SAPO-S, and SAPO-C and a simulated diffractogram of the AFI zeolite structure. The samples showed sharp reflections over the whole 2θ range, indicating that they contained a crystalline phase. SAPO-5 and SAPO-5M had an AFI structure type. SAPO-P was a mixture of two structures, AFI and CHA (Fig. S1, Supporting information). The diffractogram of SAPO-A corresponded to that of ALPO-H4 [27]. A background in the diffractogram of SAPO-A indicated the presence of amorphous material. SAPO-S and SAPO-C were of SOD and CHA structure types, respectively (Fig. S1, Supporting information). No reflections were observed in the low 2θ range, indicating that the samples did not contain regular, uniform mesopores.

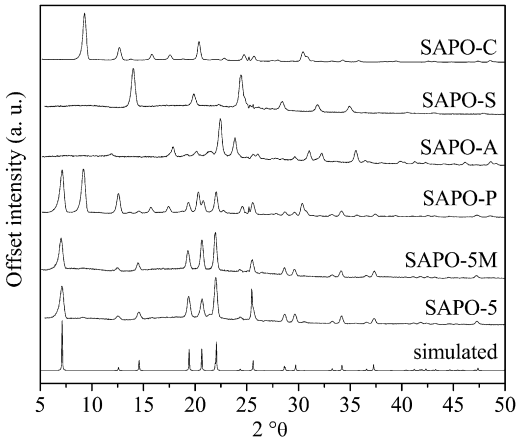

Fig. 1. XRD of SAPO-5, SAPO-5M, SAPO-P, SAPO-A, SAPO-S, and SAPO-C and the simulated pattern of AFI.

Table 1 gives the results of nitrogen physisorption, elemental analysis, and the deconvolution of ^{29}Si MAS NMR spectra. The BET and the external surface area of SAPO-5M were about 10% and 45% higher, respectively, than those of microporous SAPO-5. The micropore volumes of SAPO-5 (0.1 cm^3/g) and SAPO-5M (0.09 cm^3/g) were similar, and both were high. These values were in good agreement with those reported in the literature [28]. Furthermore, SAPO-5M had a large mesopore volume of 0.73 cm^3/g. The BET surface area and the micropore volume of SAPO-P were relatively high. This is explained by the presence of the CHA impurity. The external surface area was 47 m^2/g and the mesopore volume was only 0.06 cm^3/g, indicating only a small number of mesopores. The BET surface area of SAPO-A was 148 m^2/g, almost as large as its external surface area. Porosity was not detected. The BET surface area of SAPO-S (68 m^2/g) was low. The whole surface area of the sample was the external surface area; the sample was non-porous. This is in agreement with the results of XRD, which showed that SAPO-A and SAPO-S were of the ALPO-H4 and SOD structure type, respectively, which are dense phases. SAPO-C showed a very high surface area of 613 m^2/g and microporous volume of 0.26 cm^3/g, typical of materials of CHA structure type (SAPO-34). The external surface area of SAPO-C was very small and mesoporosity was not observed, indicating that microporous SAPO with a CHA structure was obtained. The isotherm of SAPO-5 was typical of microporous material (Fig. 2); SAPO-5M contained a hysteresis of type IV, typical of mesoporous material [29]. The shape of the hysteresis suggested presence of aggregates of platy particles with pores of different shape and size. The pore size distribution of SAPO-5M (Fig. 2, inset) showed two maxima, one at 3.8 nm, which is probably attributed to the so-called tensile strength effect [30], and a relatively broad one centered at about 12 nm, representing the mesopores.

AAS indicated that SAPO-5, SAPO-5M, SAPO-P, and SAPO-A contained a considerable amount of silicon. The deconvolution of ^{29}Si MAS NMR spectra (Fig. S2, Supporting information) revealed that, for SAPO-5, SAPO-5M, and SAPO-P, most of the silicon was in the

Table 1
Results of characterization of SAPO-5, SAPO-5M, SAPO-P, SAPO-A, SAPO-S, and SAPO-C.

Sample	BET surface area (m^2/g)	S_{ext} (m^2/g)	V_{micro} (cm^3/g)	V_{meso} (cm^3/g)	Si_{bulk}[a] (wt.%)	Si_{SAPO}[b] (wt.%)
SAPO-5	325	93	0.10	0.12	5.6	3.3
SAPO-5M	367	170	0.09	0.73	5.3	3.7
SAPO-P	441	47	0.17	0.06	4.9	3.2
SAPO-A	148	138	0	0	12	3.4
SAPO-S	68	68	0	0	n.d.[c]	n.d.
SAPO-C	613	7	0.26	0	n.d.	n.d.

[a] Determined by AAS.
[b] Si in SAPO domains determined from deconvolution of ^{29}Si MAS NMR spectra (Fig. S1, Supporting information).
[c] Not determined.

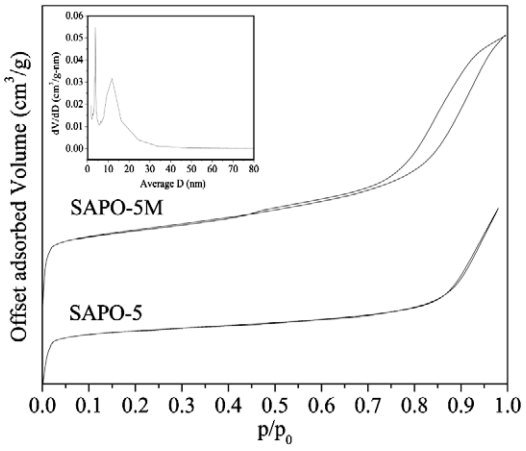

Fig. 2. Nitrogen sorption isotherms of SAPO-5 and SAPO-5M and pore size distribution of SAPO-5M.

framework (*vide infra*). Most of the silicon in SAPO-A was of extra-framework nature. However, because there were several possibilities to deconvolute the spectra, the values are significantly uncertain with regard to the silicon content in the framework.

Fig. 3 shows ^{29}Si, ^{27}Al, and ^{31}P MAS NMR spectra of H-SAPO-5 and H-SAPO-5M. SAPO consists of aluminosilicate regions with a Si(2Al, 2Si) configuration, which is also observed in zeolites [31], and of silicon-rich regions or silicon-islands [32]. These different regions result from different possibilities of substitution of aluminum and phosphorus atoms by silicon during its incorporation into the framework [33]. The ^{29}Si MAS NMR spectra (Fig. 3a) of H-SAPO-5 and H-SAPO-5M were broad and asymmetrical, indicating the presence of different silicon species. We assign the intense peak at about −90 ppm to framework silicon atoms, which were located in the aluminosilicate region of the sample [6,34]. The resonances at higher chemical shifts represented silicon located in the silicon-rich regions of H-SAPO-5 and H-SAPO-5M. Both samples showed peaks in the ^{27}Al MAS NMR spectra at around 50 and 0 ppm, corresponding to tetrahedrally and octahedrally coordinated aluminum, respectively (Fig. 3b). The mesoporous sample contained more octahedral aluminum, which could be of framework or extraframework nature. The peak at 17 ppm in the spectrum of H-SAPO-5M is attributed to pentacoordinated aluminum. ^{31}P MAS NMR spectra showed only one peak at around 30 ppm (Fig. 3c), which is attributed to phosphorus in the framework. This peak was asymmetrical and had a tail toward lower chemical shift.

Fig. 4a shows the SEM of a SAPO-5M particle, which in fact was an agglomerate of about 100 nm thin platelets. Fig. 4b–d shows TEM micrographs of SAPO-5M. Bright spots appeared due to differences in thickness (Fig. 4b), which correspond to mesopores (thickness contrast). Their diameter was between 8 and 30 nm. Their size is in a good agreement with the average pore size obtained from nitrogen physisorption. Zeolite lattice fringes were easily recognizable in micrographs of high magnification (Fig. 4c, inset). The sample contained round and tail-shaped cavities (Fig. 4c and d), which may have accommodated the porogenous template molecules.

Table 2 gives an overview of the results of TPD–TGA of *n*-propylamine, monomolecular propane cracking, and isomerization of 2-methyl-2-pentene for H-SAPO-5 and H-SAPO-5M. Both samples chemisorbed roughly the same amount of *n*-propylamine, indicating that the number of acid sites was similar. The reaction rate and the activation energy for the monomolecular cracking of propane, obtained from the slope of the Arrhenius plots (Fig. S3, Supporting information), were very similar for the microporous H-SAPO-5 and the mesoporous H-SAPO-5M, which indicates that the catalytically active sites in this reaction are the same. Assuming that in the isomerization of 2-methyl-2-pentene, the molar ratio of *trans*-3-methyl-2-pentene, obtained by methyl shift, to *trans*- and *cis*-4-methyl-2-pentene, obtained by hydrogen shift reflects the acidity, equal acidity was observed: at similar conversion of about 60%, the molar ratio was 1.3.

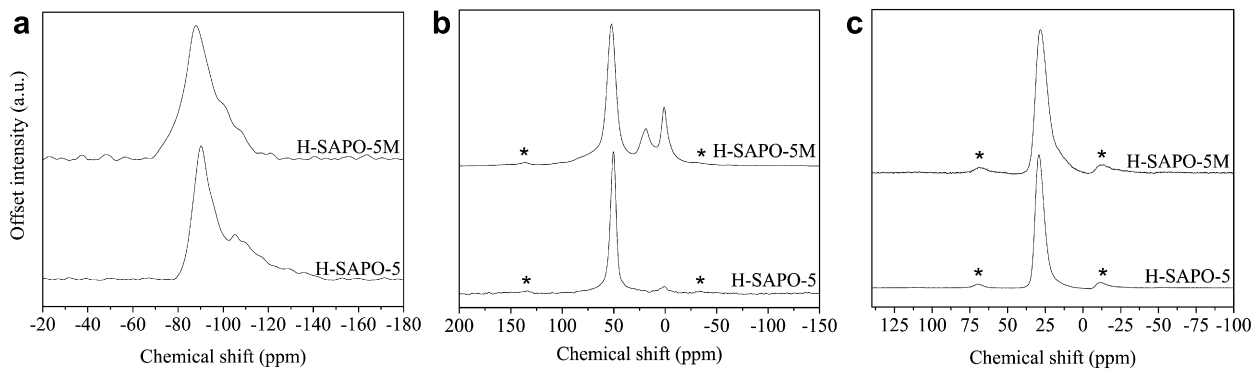

Fig. 3. ^{29}Si (a), ^{27}Al (b), and ^{31}P (c) MAS NMR of H-SAPO-5 and H-SAPO-5M, ∗ denote spinning side bands.

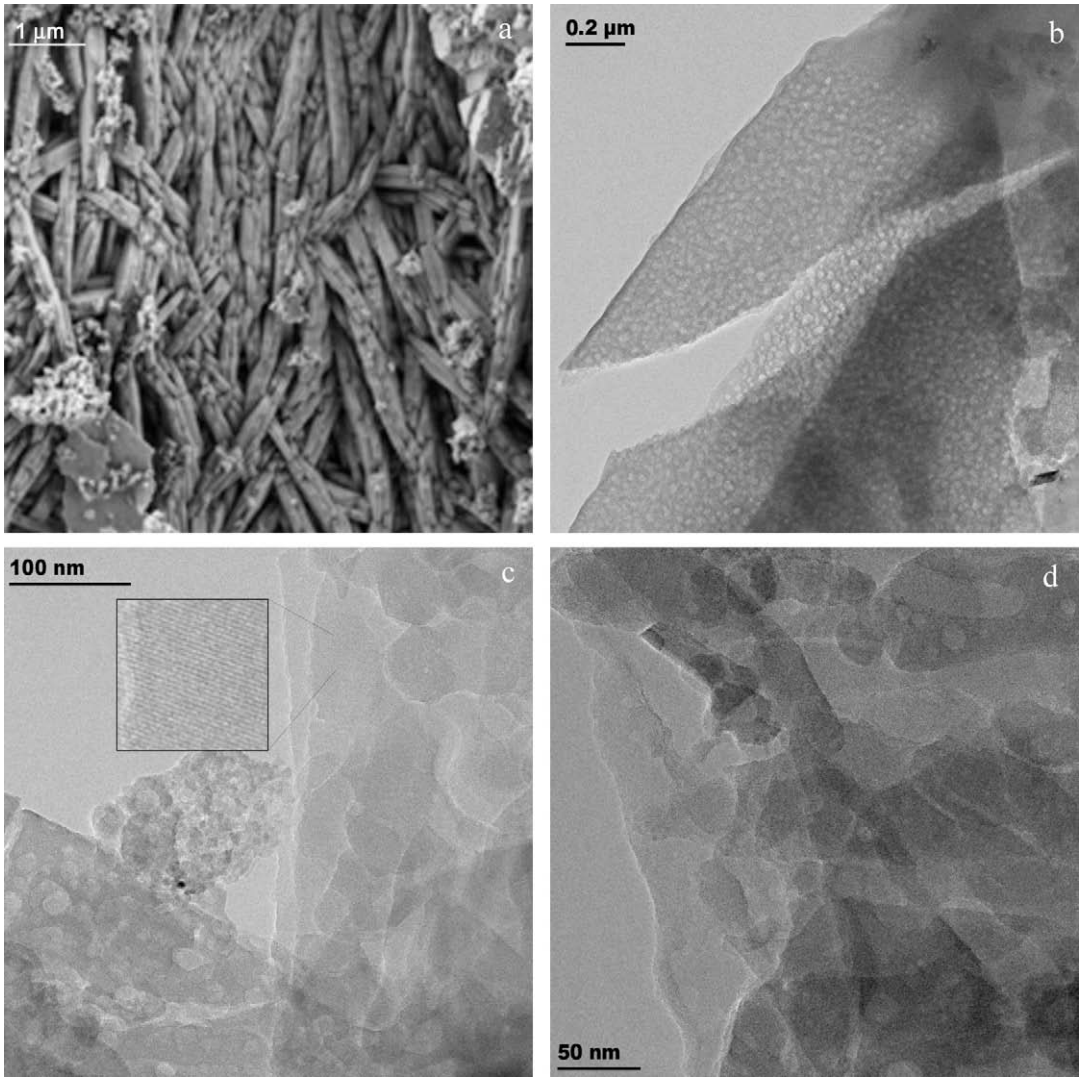

Fig. 4. SEM (a) and TEM (b–d) micrographs of SAPO-5M.

Table 2
Results of TPD–TGA, monomolecular propane cracking, and isomerization of 2-methyl-2-pentene for H-SAPO-5 and H-SAPO-5M.

Sample	$n_{n\text{-PA}}$[a] (mmol/g)	$r_{cr}^{propane}$[b] (mol/g s bar)	$E_A^{propane}$ (kJ/mol)	X_{2M2P}[c] (%)	3MP/4MP[d]
H-SAPO-5	0.79 ± 0.02	2.41×10^{-7}	189	61	1.3
H-SAPO-5M	0.83 ± 0.02	2.26×10^{-7}	188	66	1.3

[a] Mole of decomposed *n*-propylamine.
[b] Cracking rate of propane at 848 K.
[c] Conversion of 2-methyl-2-pentene.
[d] Molar ratio of 3-methyl-2-pentenes to 4-methyl-2-pentenes.

Fig. 5a shows the conversion plot in the alkylation of benzene with benzyl alcohol for H-SAPO-5, H-SAPO-5M, and H-ZSM-5. H-ZSM-5 (ZEOcat® PZ-2/50 H) was obtained from Zeochem AG, Uetikon, Switzerland. The Si/Al ratio was 25 and the BET surface area 400 m^2/g. After 3.5 h of reaction, the conversion of benzyl alcohol over H-SAPO-5M reached 98%, whereas the conversion over the microporous H-SAPO-5 was around 66%, and over H-ZSM-5 it was below 10%. Assuming that the reaction was of first-order, the reaction rates of all the samples were determined (Fig. 5b). Table 3 gives the rate constants and selectivities. The rate for H-SAPO-5M was more than three times higher than that for the microporous H-SAPO-5 and roughly 35 times higher than for H-ZSM-5. The selectivity was calculated for H-SAPO-5 and H-SAPO-5M at a conversion of 55%. The mesoporous sample showed higher selectivity to the bulkier products, dibenzyl ether and dibenzyl benzene, which indicates that the reaction took place in the mesoporous domains. Over H-ZSM-5 only diphenylmethane formed.

4. Discussion

The dual templating method, with cyclohexylamine and an organosilane with a long hydrocarbon chain, yielded a crystalline SAPO-5 with a high micro- and mesoporosity. The organosilane TPHAC is already known to act as a mesopore-directing template

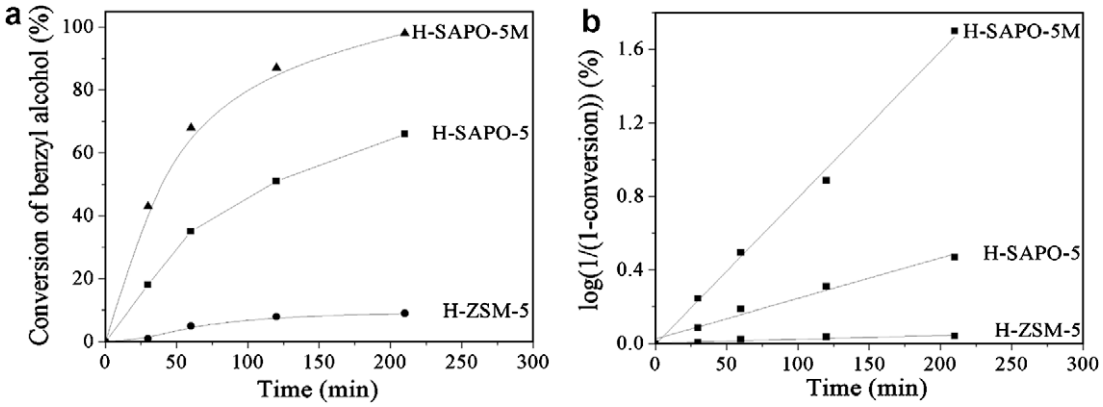

Fig. 5. Conversion of benzyl alcohol (X_{BA}) vs. time (a) and rate constant in the alkylation of benzene with benzyl alcohol (b) for H-ZSM-5 (●), H-SAPO-5 (■), and H-SAPO-5M (▲).

Table 3
Results of alkylation of benzene with benzyl alcohol (BA) over H-ZSM-5, H-SAPO-5, and H-SAPO-5M.

Sample	X_{BA}[a] (%)	k (min^{-1})	Selectivity[b] (%)		
			DPM[c]	DBE[d]	DBB[e]
H-ZSM-5	9	0.2×10^{-3}	100	0	0
H-SAPO-5	66	2.4×10^{-3}	87	11	2
H-SAPO-5M	98	7.9×10^{-3}	74	23	3

[a] After 3.5 h of reaction.
[b] At 55% conversion of BA.
[c] DPM – diphenylmethane.
[d] DBE – dibenzyl ether.
[e] DBB – dibenzyl benzene.

in the synthesis of several hierarchical zeolite structures, such as AEL [8], AFI [8], LTA [9], MFI [9,16], and MOR [35]. Materials synthesized by alternative templating procedures did not crystallize in a pure AFI structure or did not contain mesopores, indicating that, during synthesis, phase segregation may have occurred. Syntheses of mesoporous SAPO with a high silicon content with amphiphilic molecules are reported in the literature [6,7]. Amorphous or partially crystalline structures, which did not have an AFI structure, were obtained. Compared to mesoporous ZSM-5 [16] and ALPO-5 [8], synthesized in the presence of TPHAC as a template, H-SAPO-5M had a much larger mesoporous volume, although the same or even smaller amount of TPHAC was used for its synthesis. The microporous volume is in good agreement with that of hierarchical H-ALPO-5 reported in the literature [8]. The pore size of roughly 12 nm was around four times higher than that observed for hierarchical ZSM-5, suggesting a different ordering of the mesopore-directing template. As revealed by the EM images and nitrogen physisorption, the mesopores consisted of both intra- and intercrystalline voids between crystalline domains.

The crystallinity and the microporosity of the hierarchical SAPO-5M are properties typical of zeolites and zeotypes. Combined with the high silicon content in the framework, these features are responsible for the high acidity and activity of the mesoporous sample. H-SAPO-5M had a high silicon content in the SAPO domain, equal to that of H-SAPO-5. The deconvoluted ^{29}Si MAS NMR spectra (Fig. S2, Supporting information) showed peaks between −98 and −110 ppm, which are also assigned to silicon with one or two aluminum neighboring atoms. Such zeolitic domains may also be acidic and, thus, contribute to catalytic activity [36]. It is known from the literature that, with increasing amount of silicon in the synthesis gel, the content of the aluminosilicate domain increases [36]. At 0.28 equivalents of silicon in the framework, about 25% of it may have a zeolitic environment. The substitution pattern for silicon in SAPO molecular sieves is known to be sensitive to many synthesis parameters, such as total silicon content, template/Al_2O_3 ratio, P_2O_5/Al_2O_3 ratio, pH, and crystallization time, and temperature [7,37,38].

The acidity expressed by the conversion of 2-methyl-2-pentene and the 3MP/4MP ratio was similar for H-SAPO-5 and H-SAPO-5M. In comparison, over ZSM-5, the conversion was almost the same, whereas the 3MP/4MP ratio over SAPO was lower (1.3) than over ZSM-5 (1.9) [16]. The number of Brønsted acid sites and their intrinsic reactivity, determined by the TPD/TGA of *n*-propylamine and propane cracking, were similar for the micro- and the mesoporous samples. The intrinsic activation energy is a measure of acidity and equals the apparent activation energy minus the heat of reactant adsorption. The strength of the adsorption depends on the fit of the reactant within the pore: the better the fit, the higher the heat of adsorption [39]. Therefore, the size and shape of the pores, in which the reaction occurs, are the main factors in determining the cracking activity of Brønsted acid sites. For the AFI structure, the heat of adsorption was −36 kJ/mol [40], similar to that obtained for FAU (−31 kJ/mol) [41], which has a similar pore size. The identical activation barrier of propane cracking for the micro- and the mesoporous SAPO (188–189 kJ/mol) suggests equal strength of catalytically active sites, indicating that they are most probably located in the micropores of both samples. Typical values of the apparent activation energy of cracking for zeolites are between 146 kJ/mol for MFI and 165 kJ/mol for FAU [41] and for amorphous silica-alumina (ASA) between 182 and 186 kJ/mol [42]. Assuming that the active sites for propane cracking are within the microporous SAPO domain, which might be an approximation (*vide infra*), the intrinsic activation barrier in SAPO is higher than for zeolites. The activity per Brønsted acid site in propane cracking is calculated from the rate of cracking of propane and the number of Brønsted acid sites determined by TPD/TGA of *n*-propylamine. For H-SAPO-5, it was 3.05 ± 0.02 mol $(mmol\ s\ bar)^{-1}$ and for H-SAPO-5M, 2.72 ± 0.02 mol $(mmol\ s\ bar)^{-1}$.

The role of the mesopores was revealed by space-requiring alkylation of benzene with benzene alcohol. Although it has almost the same number and strength of Brønsted acid sites as its microporous analog, H-SAPO-5M was roughly three times more active than H-SAPO-5. This significant difference in catalytic activity indicates that the reaction occurs in the mesoporous domain, in agreement with the large external surface area. The presence of very bulky products also indicates that at least a part of the reaction takes place at the external surface. H-ZSM-5 showed 35 times less catalytic activity, in spite of its higher acidity and no bulky reaction products. H-ZSM-5, with an external surface area of 123 m^2/g and a BET surface area of 399 m^2/g, which are higher than that of H-

SAPO-5, showed very low activity. Therefore, most of its catalytically active sites are located in the micropores, and the external surface did not contribute significant to the reaction. The aluminosilicate domains in SAPO-5M are the most likely candidates for catalytic activity in the alkylation reaction. They are probably located at or near the external surface of the crystal.

5. Conclusion

Hierarchical SAPO-5 with a bimodal pore structure, significant content of silicon in the framework, and improved acidic properties was synthesized using an organosilane as the template. Soft template synthesis with phosphorus- and aluminum-containing molecules and an amphiphilic surfactant and hard-template synthesis with carbon pearls resulted in amorphous, impure, or dense materials. Mesoporous SAPO-5 was catalytically evaluated in monomolecular propane cracking, isomerization of 2-methyl-2-pentene, and alkylation of benzene with benzyl alcohol. Compared to the microporous analog, mesoporous H-SAPO-5 has similar acidic properties and shows a higher reaction rate in the conversion of bulky molecules. In contrast to H-ZSM-5, the external surface of H-SAPO-5 and H-SAPO-5M contributes to the alkylation reaction.

Acknowledgment

The work was supported by the Swiss National Science Foundation. Electron microscopy was performed at the Electron Microscopy of the ETH Zurich (EMEZ).

Appendix A. Supplementary material

Supplementary data associated with this article can be found, in the online version, at doi:10.1016/j.jcat.2010.03.014.

References

[1] I.I. Ivanova, N. Dumont, Z. Gabelica, J.B. Nagy, E.G. Derouane, F. Ghigny, in: R. von Balmoos, J.B. Higgins, M.M.J. Treacy (Eds.), Proceedings of the 9th International Zeolite Conference, Montreal, Canada, 1992, Butterworth-Heinemann, Boston, MA, 1993, p. 327.
[2] R.J. Pellet, G.N. Long, J.L. Rabo, P.K. Coughlin, US Patent 4 740 650, 4, 1988.
[3] R.J. Pellet, G.N. Long, J.L. Rabo, P.K. Coughlin, US Patent 4 751 340, 6, 1988.
[4] U. Sridevi, N.C. Pradhan, B.K.B. Rao, C.V. Satyanarayana, B.S. Rao, Catal. Lett. 79 (2002) 69.
[5] V. Huela, N. Bilba, M. Lupascu, E. Dumitriu, D. Nibou, S. Lebaili, H. Kessler, Micropor. Mater. 8 (1997) 201.
[6] B. Chakraborty, A.C. Pulikottil, B. Viswanathan, Appl. Catal. A: Gen. 167 (1998) 173.
[7] X.S. Zhao, G.Q. Lu, A.K. Whittaker, J. Drennan, H. Xu, Micropor. Mesopor. Mater. 55 (2002) 51.
[8] M. Choi, R. Srivastava, R. Ryoo, Chem. Commun. (2006) 4380.
[9] M. Choi, H.S. Cho, R. Srivastava, C. Venkatesan, D.-H. Choi, R. Ryoo, Nat. Mater. 5 (2006) 718.
[10] Y. Wan, D. Zhao, Chem. Rev. 107 (2006) 2822.
[11] K. Egeblad, C.H. Christensen, M. Kustova, C.H. Christensen, Chem. Mater. 20 (2008) 946.
[12] W.J. Roth, Stud. Surf. Sci. Catal. 168 (2007) 221.
[13] J. Perez-Ramirez, C.H. Christensen, K. Egeblad, C.H. Christensen, J.C. Groen, Chem. Soc. Rev. 37 (2008) 2530.
[14] F.-S. Xiao, Catal. Surv. Asia 8 (2004) 151.
[15] H. Wang, T.J. Pinnavaia, Angew. Chem. Int. Ed. 45 (2006) 45.
[16] Y. Sun, R. Prins, Appl. Catal. A 336 (2007) 11.
[17] M. Tiemann, M. Fröba, Chem. Commun. (2002) 406.
[18] V.N. Shetti, J. Kim, R. Srivastava, M. Choi, R. Ryoo, J. Catal. 254 (2008) 296.
[19] L. Xu, S. Wu, J. Guan, H. Wang, Y. Ma, K. Song, H. Xu, H. Xing, C. Xu, Z. Wang, Q. Kan, Catal. Commun. 9 (2008) 1272.
[20] X. Meng, F. Nawaz, F.-S. Xiao, Nano Today 4 (2009) 292.
[21] W.O. Haag, R.M. Dessau, R.M. Lago, Stud. Surf. Sci. Catal. 60 (1991) 255.
[22] T.F. Narbeshuber, H. Vinek, J.A. Lercher, J. Catal. 157 (1995) 388.
[23] B. Xu, F. Rotunno, S. Bordiga, R. Prins, J.A. van Bokhoven, J. Catal. 241 (2006) 66.
[24] G.M. Kramer, G.B. McVicker, Acc. Chem. Res. 19 (1986) 78.
[25] K.J. Huttinger, M.F. Jung, Chem. Ing. Tech. 61 (1989) 258.
[26] K. Egeblad, M. Kustova, S.K. Klitgaard, K. Zhu, C.H. Christensen, Micropor. Mesopor. Mater. 101 (2007) 214.
[27] D.M. Poojary, K.J. Balkus, S.J. Riley, B.E. Gnade, A. Clearfield, Micropor. Mater. 2 (1994) 245.
[28] J.A. Martens, P.J. Grobet, P.A. Jacobs, J. Catal. 126 (1990) 299.
[29] F. Rouquerol, J. Rouquerol, K. Sing, Adsorption by Powders and Porous Solids: Principles, Methodology and Applications, Academic Press, London, 1999.
[30] S.J. Gregg, K.S.W. Sing, Adsorption, Surface Area and Porosity, Academic Press, London, 1982.
[31] H.-X. Li, M.J. Annen, C.-Y. Chen, J.P. Arhancet, M.E. Davis, J. Mater. Chem. 1 (1991) 79.
[32] H.-X. Li, M.E. Davis, J. Phys. Chem. 96 (1992) 331.
[33] H.O. Pastore, S. Coluccia, L. Marchese, Annu. Rev. Mater. Res. 35 (2005) 351–395.
[34] J.A. Martens, C. Jansens, P.J. Grobet, H.K. Beyer, P.A. Jacobs, in: P.A. Jacobs, R.A. van Santen (Eds.), Zeolites: Facts, Figures, Future, Elsevier Science Publishers, Amsterdam, 1989, p. 215.
[35] X. Li, R. Prins, J.A. van Bokhoven, J. Catal. 262 (2009) 257.
[36] St.T. Wilson, in: H. van Bekkum, E.M. Flaningen, P.A. Jacobs, J.C. Jansen (Eds.), Introduction to Zeolite Science and Practice, Elsevier, Amsterdam, 2001, p. 249.
[37] L. Wang, C. Guo, S. Yan, X. Huang, Q. Li, Micropor. Mesopor. Mater. 64 (2003) 63.
[38] R. Roldan, M. Sanchez-Sanchez, G. Sankar, F.J. Romero-Salguero, C. Jimenez-Sanchidrian, Micropor. Mesopor. Mater. 99 (2007) 288.
[39] F. Eder, M. Stockenhuber, J.A. Lercher, J. Phys. Chem. B 101 (1997) 5414.
[40] F. Eder, Thermodynamics and Sitting of Alkane Sorption in Molecular Sieves, Dissertation, ISBN 90-3650861-4, Enschede, The Netherlands, 1996, p. 92.
[41] B. Xu, C. Sievers, S.B. Hong, R. Prins, J.A. van Bokhoven, J. Catal. 244 (2006) 163.
[42] B. Xu, C. Sievers, J.A. Lercher, J.A. Rob van Veen, P. Giltay, R. Prins, J.A. van Bokhoven, J. Phys. Chem. C 111 (2007) 12075.